Am J Physiol Lung Cell Mol Physiol 321: L1206–L1214, 2021.
First published November 17, 2021; doi:10.1152/ajplung.00328.2021

american physiological society

AMERICAN JOURNAL OF PHYSIOLOGY
LUNG CELLULAR AND MOLECULAR PHYSIOLOGY

INNOVATIVE METHODOLOGY

A new anesthesia protocol enabling longitudinal lung-function measurements in neonatal rabbits by micro-CT

Erica Ferrini,[1]* Ludovica Leo,[2]* Luisa Corsi,[3] Chiara Catozzi,[3] Fabrizio Salomone,[3] Luisa Ragionieri,[1] Francesca Pennati,[4] and Franco Fabio Stellari[3]

[1]*Department of Veterinary Science, University of Parma, Parma, Italy;* [2]*Department of Medicine and Surgery, University of Parma, Parma, Italy;* [3]*Chiesi Farmaceutici, S.p.A., Corporate Pre-Clinical Research and Development, Parma, Italy; and* [4]*Department of Electronics, Information, and Bioengineering, Politecnico di Milano, Milan, Italy*

Abstract

Micro-computed tomography (micro-CT) imaging is an emerging technology with many applications in small animals, for example, the study of pulmonary diseases, although clear guidelines and critical mass of evidence are still missing in the preclinical literature. The neonatal rabbit is a valuable model for studying pulmonary development. However, the longitudinal monitoring of lung function by micro-CT can be challenging. Distinctive datasets corresponding to the end-inspiration and end-expiration phases need to be generated and analyzed to derive lung-functional parameters. The quality of CT scans and the reliability of parameters obtained remain highly dependent on the anesthesia protocol used. Three different anesthetic protocols were tested. The combination of dexmedetomidine 0.25 mg/kg injected intraperitoneally followed by 1% isoflurane was found to facilitate CT imaging at 4 and 11 days after birth. Contrarily, isoflurane and ketamine-xylazine were found unsuitable and thus not investigated further. Total lung volumes significantly increased at *day 11* compared with baseline in both respiratory phases, whereas lung tissue remained constant. As expected, functional residual capacity, air-to-tissue ratio, and minute ventilation were significantly increased at *day 11* in each animal. Those parameters were correlated with inspiratory capacity, compliance, elastance, and resistance of both respiratory system and tissue component, as measured by flexiVent. Lung development was also evaluated by histomorphometric analyses. In conclusion, we have identified a safe and suitable anesthesia protocol for micro-CT imaging in neonatal rabbits. Moreover, the possibility to longitudinally measure lung function in the same subject dramatically reduced the intraexperimental variability.

anesthesia; longitudinal study; lung function; micro-CT imaging; term rabbit pups

INTRODUCTION

Micro-computed tomography (micro-CT) imaging is rapidly emerging as a noninvasive technology with a broad range of applications in different fields of research. In lung imaging, in particular, micro-CT allows the longitudinal quantification of air and tissue parameters, highlighting parenchymal changes caused by a progressive disease or reflecting lung development (1, 2).

High-resolution-computed tomography (HRCT) is an invaluable tool for the assessment of several lung disorders in clinical practice, with clear diagnostic guidelines (3–5). However, in preclinical studies, the critical mass of evidence is still missing with still scarce micro-CT data and uncertain procedures either for extracting quantitative information from CT images or for selecting the most suitable anesthetic protocol.

In the literature, most of lung measurements rely on a unique respiratory phase, usually consisting of the end-expiration phase where free-breathing animals lie still for most of the acquisition time (2). This represents, however, only a static view of what occurs inside the lung, precluding any dynamic evaluation over time.

Lung-function parameters can be only extracted by analyzing two distinctive datasets corresponding to the main respiratory phases, i.e., the end-inspiration and end-expiration phases, doubling the postprocess time and data storage.

Although the recent implementation of respiratory gating algorithms can provide two distinctive datasets, the quality of scans remains strictly dependent on the anesthesia protocol used (6, 7). For this reason, optimal anesthesia for image acquisition is essential. It is crucial that anesthesia is safe, with the shortest recovery time to allow multiple measures on the same subject; it should minimize undesirable body movements, thus avoiding motion-related artifacts, and should stabilize the breathing rate to permit the proper reconstruction of the two datasets.

* E. Ferrini and L. Leo contributed equally to this work.
Correspondence: F. F. Stellari (fb.stellari@chiesi.com).
Submitted 4 August 2021 / Revised 27 October 2021 / Accepted 30 October 2021

The neonatal rabbit has been extensively reported as a useful model for studying lung physiology and pathophysiology (8–13), providing many opportunities for accurate investigation of lung development in a small animal model (2). However, their size and anatomical/physiological characteristics make them extremely vulnerable to any hypothermia, rapid desaturation, and hypoxemia that may occur during anesthesia (14).

In this study, we intended to identify a safe and reliable anesthetic protocol to facilitate longitudinal quantification of lung function in newborn term rabbits by micro-CT at 4 and 11 days after birth.

By referring to the current bronchopulmonary dysplasia (BPD) model (2), *days 4* and *11* after term birth (*day 31* of gestation) correspond to *days 7* and *14* after preterm birth (*day 28* of gestation), that coincide with the time of BPD diagnosis in neonates (15).

MATERIALS AND METHODS

Animals

Time-mated New Zealand White rabbits were obtained from Charles River Laboratories (France). Pregnancy was confirmed with ultrasound examinations 12–14 days after artificial insemination at the supplier's facility. Animals were maintained in the research facility receiving food and water ad libitum until natural delivery of pups occurred (*day 31*).

After birth, term rabbit pups were then placed on soft bedding inside an incubator under controlled conditions of normoxia (21% oxygen) and temperature (32°C). From *day 4* (baseline timepoint), the body weight of pups was daily noted to monitor their development in term of % of gain with respect to baseline and determine the amount of food to be provided twice daily to each pup (Supplemental Fig. S1, *A* and *B*; see https://doi.org/10.6084/m9.figshare.15098469).

Six rabbit neonates were used for testing two anesthetic protocols, three for isoflurane (Iso) alone and three for ketamine (Keta) + xylazine (Xyla), respectively. Then, six further rabbit pups were used to test the new combination of Dex and Iso. They were longitudinally monitored by micro-CT at 4 and 11 days after birth, subjected to flexiVent analysis at the end point, and finally euthanized for lung excision ($n = 6$ at *day 11*). Other six pups, instead, were euthanized at *day 4* only to provide some histological observations of early lung development.

Ethical Statement

All animal experiments described herein were authorized by the official competent authority and approved by the Intramural Animal-Welfare Committee for Animal Experimentation of Chiesi Farmaceutici and in compliance with the European Directive 2010/63 UE, Italian D.Lgs 26/2014, the revised *Guide for the Care and Use of Laboratory Animals* (16) and with the Animal Research: Reporting of In Vivo Experiments (ARRIVE) guidelines (17). The experimental protocol was approved by the internal AWB (Animal Welfare Body) and authorized by the Italian Ministry of Health (Protocol No. 809/2019-PR).

Anesthesia Protocol

Three different anesthetic protocols were evaluated on newborns at *days 4* and *11*: Iso at 4% in oxygen in saturated chamber (IsoFlo, Zoetis, Inc., New Jersey), Keta (Lobotor, ACME, Cavriago, Reggio Emilia, Italia), and Xyla (Rompun, Bayer, Germany) intraperitoneally injected and the combination of Dex (Dexdomitor, Zoetis, Inc.) intraperitoneally injected followed by exposure to 1% Iso. All details were reported in Table 1.

Dex was injected intraperitoneally (0.25 mg/kg). Thereafter, neonates were supplied with oxygen until 100% saturation was reached to reduce the risk of hypoxemia during image acquisition.

Pups were then positioned inside the CT scan and anesthetized with 1% Iso in oxygen using a facemask. The homemade facemask was designed to fit snugly on the muzzle of the rabbit pup without obstructing its mouth or nose and minimizing the dead space to avoid rebreathing of carbon dioxide (Supplemental Fig. S2*A*; see https://doi.org/10.6084/m9.figshare.15099966).

After each image acquisition, and 20 min after Dex administration, atipamezole hydrochloride (Antisedan, Zoetis, Inc.) 1 mg/kg was subcutaneously injected to facilitate the recovery time, completely displacing Dex from α_2-agonist receptors.

During all procedures, pups were kept at 32°C in a warming system (Mini Thermacage, Datesand group, Envigo, San Pietro al Natisone, Udine, Italia) except for during the scan period and received 100% oxygen during the recovery time.

Measurements of body temperature (°C), breathing rate per minute, heart beats per minute (beats/min), and blood oxygenation (%O_2) were recorded before and after premedication, after micro-CT imaging, and after recovery in newborn rabbits anesthetized with the combination Dex plus Iso, since neither isoflurane alone nor Keta + Xyla protocols were investigated further (Supplemental Table S1; see https://doi.org/10.6084/m9.figshare.15101181). Breathing and heart rates and blood oxygenation were recorded by

Table 1. *Anesthetic protocols*

Days after Birth	Pups, *n*	Anesthesia	Dose	Time before Imaging, Min*	Recovery Time, Min#
4	3	Iso	4%	>30	NA
11	3	Iso	4%	>30	NA
4	1	Keta + Xyla	10 + 5 mg/kg + 10 + 5 mg/kg	47	95
4	2	Keta + Xyla	20 + 10 mg/kg	13 ± 5	115 ± 10
11	2	Keta + Xyla	20 + 10 mg/kg	5 ± 0.5	100 ± 6
4	6	Dex + Iso	0.25 mg/kg + 1%	9 ± 1	30 ± 5
11	6	Dex + Iso	0.25 mg/kg + 1%	9 ± 1	28 ± 3

Values are means ± SD. Dex, dexmedetomidine; Iso, isoflurane; Keta, ketamine; NA, not available; Xyla, xylazine. *Time required to start micro-CT acquisition. #Time required to a complete restoration of pedal withdrawal reflex and mobility of the pup.

MouseOx Plus Pulse Oximeter with a paw sensor (STARR-Link, Ugo Basile, Varese, Italy).

A thermal camera (FLIR E86-EST handheld, Teledyne FLIR, Wilsonville, OR) was used to capture external temperatures during each imaging session, as reported in some representative images displayed in Supplemental Fig. S2*B*.

All injectable anesthetics were freshly prepared in saline, at the desired working concentration, at the beginning of each imaging session.

Micro-CT Lung Imaging

Lung imaging was performed with Quantum GX Micro-CT (PerkinElmer). Images were acquired with the following parameters: X-ray tube voltage 90 KV, X-ray tube current 88 μA over a total angle of 360° for a total scan time of 4 min. The "high-resolution" scan mode generated one three-dimensional (3-D) dataset with 90-μm isotropic reconstructed voxel size and was used to scan pups sedated with Iso. In pups sedated with Keta + Xyla and Dex + Iso anesthesia, images were acquired using the "high-speed" modality with an intrinsic retrospective two-phase respiratory gating technique resulting in two 3-D datasets that corresponded to the two different phases of the breathing cycle (inspiration and expiration). The same field of view and resolution were maintained between the two different timepoints.

Airways and total lung volumes were semiautomatically segmented using Perkin Elmer Analyze software (Analyze 12.0; Copyright 1986–2017, Biomedical Imaging Resource, Mayo Clinic, Rochester, MN). Micro-CT images were rescaled into Hounsfield units (HU), setting −1,000 HU as the density of air and 0 HU as the density of water. All data presented for each pup refer to both end-inspiratory (P01) and end-expiratory (P02) phases. Mean lung attenuation (MLA) was extracted from each rescaled HU image to assess air and tissue contents in the lung. Other functional parameters of interest were derived (18), i.e., the functional residual capacity (FRC, *Eq. 1*) as the volume of air (mm^3) at the end of the expiratory phase, air-to-tissue ratio (ratio, *Eq. 2*) at the end-inspiratory phase, and the tidal volume (V_t, *Eq. 3*) as the amount of air exchanged between inspiration and expiration (mm^3), as reported in Table 2. A python script (Python, version 3.8.5) was generated to estimate the breathing rate for each pup at both timepoints. During the 4 min of CT acquisition, inspiratory peaks were recorded and stored in a .csv file as amplitude values over time. The python algorithm counted the number of peaks and quantified the breathing rate per minute by dividing for the scan time.

The minute ventilation (mm^3/min) was also calculated by multiplying the tidal volume (mm^3/breath) for respiratory rate (breaths/min) (*Eq. 4*), representing a dynamic measurement of ventilation degree and then normalized on animal body weight (mm^3/min·kg).

Terminal Lung-Function Measurements

Invasive lung-function testing was performed using the forced oscillation technique with the flexiVent system (SCIREQ, Canada) on six neonatal rabbits at *day 11* after micro-CT lung imaging. The pups were anesthetized with an intraperitoneal administration of ketamine (35 mg/kg) and xylazine (6 mg/kg). Pups were then tracheostomized by an 18-gauge metal needle and connected to the volume-controlled mechanical ventilator set at tidal volume 10 mL/kg, frequency of 120 breaths/min, and positive end-expiratory pressure (PEEP) of 3 cmH_2O. The following parameters were measured: total inspiratory capacity (IC), airway resistance (R_n), lung tissue damping (tissue resistance, G), and lung tissue elastance (H) using Primewave-8 forced oscillation; static compliance (C_{st}) using the pressure-volume curve; and dynamic compliance (C_{rs}), elastance (E_{rs}), and resistance (R_{rs}) using Snapshot-120 perturbation.

Three consecutive measurements were performed until a coefficient of determination >0.95 was obtained, confirming consistent and acceptable measures. The average of these three measurements was used for the analysis.

Histomorphometric Analysis

Lung samples of pups, previously anesthetized with Dex + Iso and then subjected to longitudinal CT imaging, were collected after CT acquisition at *day 11* after birth (n = 6). Other pups (n = 6) were euthanized 4 days after birth for histological evaluations at this timepoint of observation.

All pups were euthanized with a pentothal sodium overdose before lung harvesting. Lungs were completely excised and fixed with 10% buffered formalin (Sigma-Aldrich, Germany) for at least 4 h under constant pressure (25 cmH_2O). After 48 h of formalin fixation, lung samples were dehydrated in graded alcohol solutions, xylene clarified, and paraffin-embedded with the dorsal surface of the slice down. Five-micrometer thick sections were obtained using a rotary microtome and stained with hematoxylin and eosin (H&E). Histological slides were acquired as whole slide images (WSI) by digital slide scanner (Nanozoomer S-60, Hamamatsu, Japan). The histomorphometric parameters of tissue density (TD) and air content (AC) were then semiautomatically determined using a customized application developed with Visiopharm image analysis software (Hoersholm, Denmark). Applying a threshold-based mask on lung section, it was possible to distinguish objects of interest (tissue or air) from

Table 2. *Densitometric-based calculations of lung-function parameters*

Parameter	Equation
FRC	(*Eq. 1*) $FRC\ (mm^3) = V_{P02}(mm^3)\frac{MLA_{P02}(HU)}{Air\ (HU)}$
A/T	(*Eq. 2*) $Ratio = \frac{Air_{P01}(mm^3)}{Tissue_{P01}(mm^3)}$ $\quad Air_{P01}(mm^3) = V_{P01}(mm^3)\frac{MLA_{P01}(HU)}{Air\ (HU)}$ $\quad Tissue_{P01}(mm^3) = V_{P01}(mm^3) - Air_{P01}(mm^3)$
V_t	(*Eq. 3*) $V_t\ (mm^3/breath) = Air_{P01} - FRC$
Minute ventilation	(*Eq. 4*) $Minute\ ventilation = V_t\ (mm^3/breath) \times respiratory\ rate\ (breaths/min)$

A/T, air-to-tissue ratio; FRC, functional residual capacity; HU, Hounsfield units; MLA, mean lung attenuation; P01, end-inspiratory phase; P02, end-expiratory phase; V_t, tidal volume.

background (areas of exclusion). The stained tissue area of the WSI was measured excluding air spaces, bronchi, and blood vessels and including otherwise cells and nuclei in the density mask. The TD was quantified as percentage of stained area on the total selected area. AC was measured using a white threshold and calculating the percentage of area occupied by air on the lung total area.

The radial alveolar count (RAC) parameter was manually measured in H&E-stained sections, using the Hamamatsu viewer, by drawing a perpendicular line from the lumen of the terminal bronchiole to the nearest connective tissue septum or pleural margin, and the number of air sacs or alveoli crossed by this line was counted (19–22).

Statistical Analysis

Statistical analyses were performed using Prism 8 software (GraphPad Software Inc., San Diego, CA). All data are expressed as means ± SD. Two-way ANOVA followed by Tukey's test was performed to analyze the longitudinal assessment of air and tissue inside lungs by micro-CT and histology. Micro-CT functional parameters and histological quantifications of RAC at *day 11* were compared with results at *day 4* using two-tailed paired *t* test. A $P < 0.05$ was considered statistically significant. Finally, a Spearman matrix was generated to evaluate the relationship between flexiVent data and micro-CT functional parameters ($R_{Spearman}$ data were reported corresponding to each correlation).

RESULTS

Anesthesia Protocols

Gas isoflurane.

Gas isoflurane, a common inhaled agent for in vivo imaging applications (1), was initially applied. An adequate sedation before starting image acquisition required 30 min of exposure to isoflurane and a scaling up to 4% concentration. This anesthesia produced an evident depression of tidal breathing associated with struggling and breath holding during gas administration, even at lower concentrations. Thus, neonatal rabbits were imaged using the high-resolution scan mode without the respiratory gating. As images were acquired without respiratory gating, the breathing rate could not be recorded. A unique 3-D dataset for each pup was generated with this modality representing an average condition between the inspiratory and the expiratory phase. Representative 2D projections (Fig. 1*A*) clearly highlighted body motion artifacts (red arrowheads) and heartbeat (blue arrowhead). These distortions and the impossibility of separating the inspiratory and expiratory phases precluded both functional analysis and the correct densitometric evaluation of lung aeration compartments at both timepoints of observation.

Ketamine and xylazine.

Initially, one neonatal rabbit was intraperitoneally injected with 10 mg/kg Keta + 5 mg/kg Xyla at *day 4*, but this dose was insufficient to induce sedation and a second injection with the same concentrations was necessary. The dose 20 mg/kg Keta + 10 mg/kg Xyla provoked a complete relaxation of the pups in few minutes but with long recovery times (Table 1), which drastically increased the risk of hypothermia, respiratory depression, and dyspnea. One pup died during the recovery period.

During micro-CT acquisition, the breathing pattern was recorded (Supplemental Fig. S3*Ai*; see https://doi.org/10.6084/m9.figshare.15100893) revealing constant low rates and long end-expiration phases, thus altering the normal breathing rate and the following functional analyses.

The Keta + Xyla combination was assayed at *day 11* in the two remaining pups, producing the same problems observed at *day 4* (Supplemental Fig. S3*Aii*). Although many issues emerged with this anesthesia protocol (i.e., long recovery times and altered breathing rate), imaging procedures and the reconstruction of two distinctive datasets representing the end-inspiration (P01) and end-expiration (P02) phases could be performed at *days 4* and *11* (Fig. 1*B*, *i* and *ii*, respectively).

Dexmedetomidine plus Isoflurane

The premedication of newborn rabbits with dexmedetomidine, an α_2-agonist often used in veterinary practice, proved useful in alleviating stress and significantly decreasing the amount of isoflurane required for induction and maintenance of anesthesia. Dex was intraperitoneally

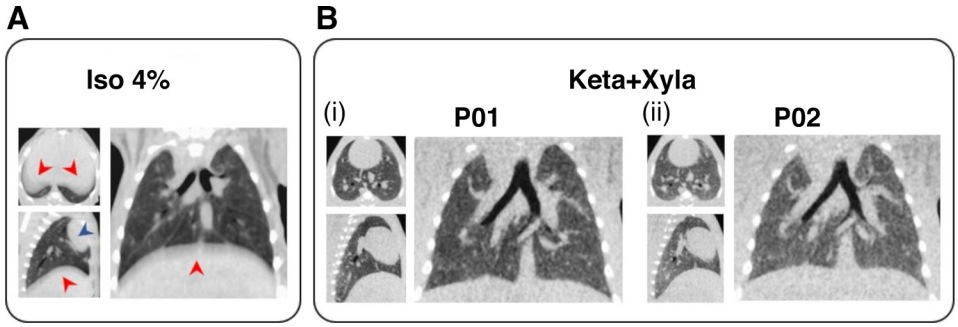

Figure 1. Pilot study: gas vs. injectable anesthesia. Representative micro-CT 2-D slides of rabbit neonates' lungs acquired after anesthesia based on gas Iso ($n = 3$; *A*) or injectable Keta + Xyla ($n = 3$; *B*). *A*: apnea induced by the gaseous agent precluded the use of respiratory gating strategy and only an average image could be obtained, affected by motion artifacts due to diaphragm (red arrowheads) and heart (blue arrowhead) movements. *B*: the injectable combination, instead, allowed the reconstruction of two distinct datasets, the end-inspiration (P01, *i*) and end-expiration (P02, *ii*) phases. CT, computed tomography; Dex, dexmedetomidine; Iso, isoflurane; Keta, ketamine; P01, end-inspiratory phase; P02, end-expiratory phase; 2-D, two-dimensional; Xyla, xylazine.

administered at 0.25 mg/kg in six rabbit pups 4 and 11 days after birth (Table 1). Five minutes after injection, the pups seemed relaxed, but they continued to react to stimulation of the pedal withdrawal reflex. The pups were positioned on micro-CT bed support and 1% Iso was supplied by a home-made facemask (Supplemental Fig. S2*A*). Complete muscle relaxation was reached 1 min before starting image acquisition. The breathing rate remained constant during the 4 min of acquisition at both *days 4* and *11*, as shown in the two representative graphs in Supplemental Fig. S3*B*, *i* and *ii*, respectively. Moreover, amplitude of peaks and rates were higher than those registered with Keta + Xyla (Supplemental Fig. S3*A*, *i* and *ii*) and were unchanged throughout the whole imaging sessions (Supplemental Table S1), suggesting that premedication and anesthesia did not negatively impact respiration. A comparable number of projections registered during inspiratory and expiratory phases was a substantial aid to generating reliable P01 and P02 datasets. As reported in Fig. 2, *A* and *B*, the image quality of the reconstructed datasets was improved, better than under the Keta + Xyla protocol, and free from motion-related artifacts.

External temperature, heart rate, and oxygenation during each imaging session were measured and reported in Supplemental Table S1. At both timepoints, a slight decrease in body temperature was observed (<1°C) especially after CT imaging. Breathing rates were not substantially influenced by anesthesia, whereas Dex administration displayed some effects on heart rate, which significantly slowed down (from 292 ± 7 to 223 ± 32 beats/min at *day 4*, $P < 0.01$; from 325 ± 21 to 213 ± 32 at *day 11*, $P < 0.05$). However, blood oxygenation never dropped below 98%.

Thus, Dex plus Iso resulted in a safe anesthesia protocol for neonatal rabbits, with short recovery times consistent with optimal animal welfare and suitable for longitudinal micro-CT imaging.

Longitudinal Measurement of Lung Function by Micro-CT

The six rabbit pups anesthetized with Dex + Iso were longitudinally monitored by micro-CT. Representative transversal and coronal lung micro-CT scans (either P01 or P02 phases) of the same subject, on *days 4* and *11*, are shown in Fig. 2, *A* and *B*.

Body volumes and lungs were increased at *day 11* compared with baseline (Supplemental Fig. S1, *A* and *B*). As expected, body weight increased by nearly 40% in the week between *days 4* and *11*, from 71 ± 15 up to 98 ± 18 g. Total lung volumes were longitudinally quantified either in P01 or P02 phases (Fig. 2*C*). On *day 4*, lung volumes were 2,400 ± 360 mm^3 in P01 and 1,700 ± 310 mm^3 in P02 and significantly increased by 11 days up to 3,830 ± 800 mm^3 in P01 ($P < 0.001$) and 3,390 ± 780 mm^3 in P02 ($P < 0.01$).

The lungs appeared darker at *day 11* compared with *day 4*, both at P01 and P02. Mean attenuation values were −445 ± 58 HU in P01 and −370 ± 68 HU in P02 on *day 4* and −575 ± 21 HU in P01 and −518 ± 25 HU in P02 on *day 11*. Air content significantly increased (black box) either in P01 or P02 phases at *day 11* compared with *day 4* ($P < 0.001$), whereas the tissue component remained constant in this stage of development (Fig. 2*C*).

Air-to-tissue ratio measured at the end of inspiration was significantly higher at *day 11* compared with baseline ($P < 0.01$, Fig. 2*D*), since the amount of air was significantly increased, whereas lung tissue was stable over time.

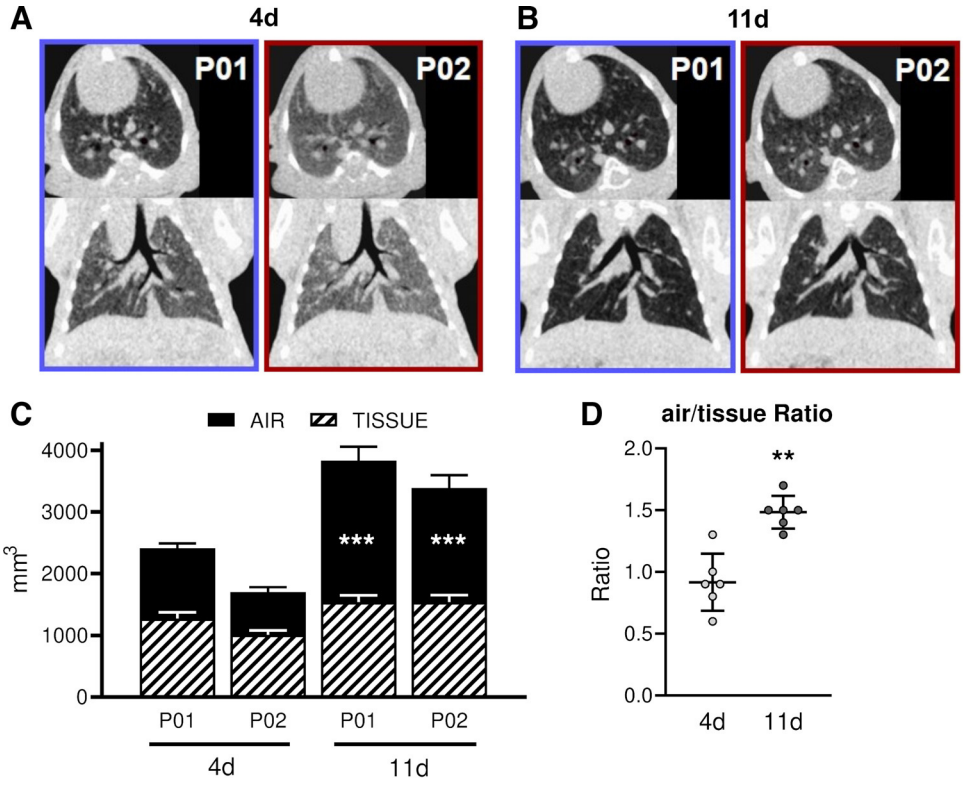

Figure 2. Low concentrations of Dex + Iso allow longitudinal and reliable micro-CT lung scans in rabbit pups. $n = 6$ newborn rabbits were premedicated using 0.25 mg/kg Dex and anesthetized with 1% Iso in oxygen. Both P01 and P02 datasets generated at *day 4* (*A*) or *day 11* (*B*) were reconstructed and analyzed. *A* and *B*: some representative transversal and coronal slides of pups' lung at the end of inspiration and expiration phases. The following quantification of air and tissue in the lung provided an important description of lung development (*C*), such as the assessment of air-to-tissue ratio (*D*). Changes in air and tissue components (mm^3) from 4 to 11 days were compared using a two-way ANOVA followed by Tukey's test (***$P < 0.001$). A paired *t* test was used to compare variations in air-to-tissue ratio between the two timepoints (**$P < 0.01$). CT, computed tomography; Dex, dexmedetomidine; Iso, isoflurane; P01, end-inspiratory phase; P02, end-expiratory phase.

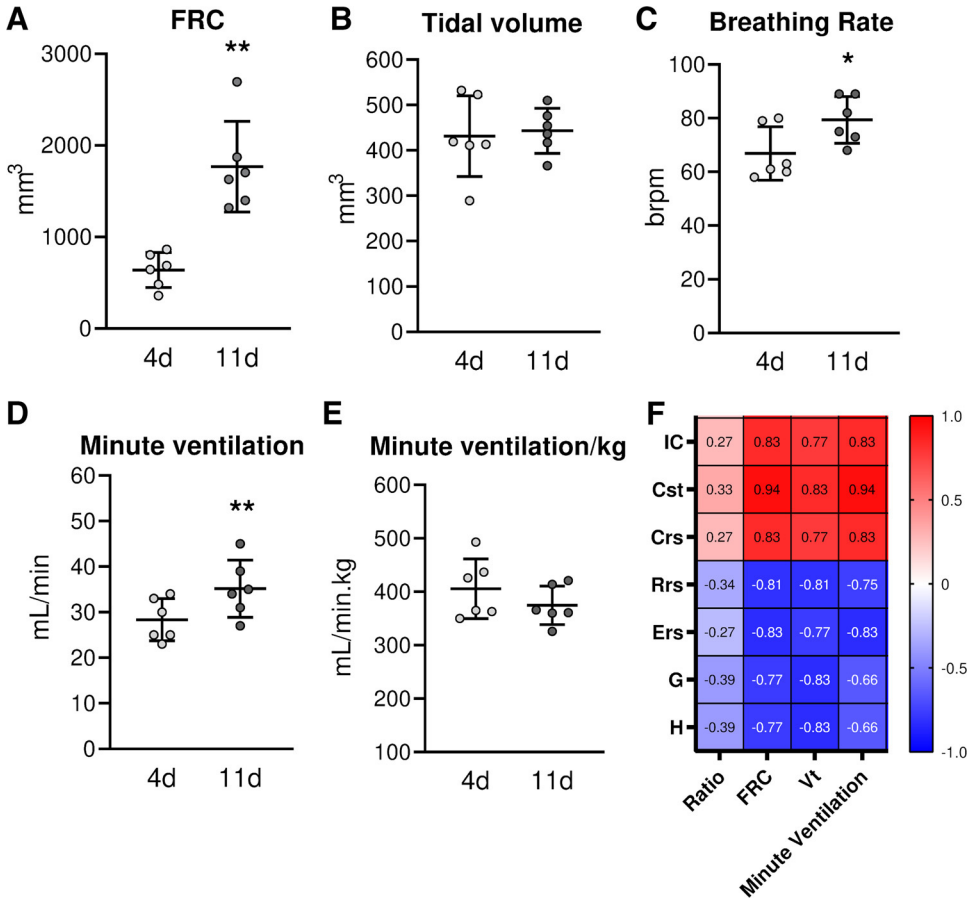

Figure 3. Lung-function measurements by micro-CT imaging: a 4-D analysis of ventilation degree. $n = 6$ term rabbit pups were longitudinally scanned by micro-CT at the two timepoints, 4 and 11 days after birth. For each pup FRC (*A*), tidal volume (*B*), breathing rates (*C*), minute ventilation (*D*), and minute ventilation/kg (*E*) were calculated. *A*: FRC corresponded to the air content in the lung at the end of expiration. *B*: the tidal volume was measured as the difference between air content in inspiration and expiration phase. The number of respiratory peaks (*C*) recorded during 4 min of CT acquisition was automatically extracted. *D*: minute ventilation was calculated as mm^3 air exchanged in the lung in a minute and was also expressed normalized by pup body weight (*E*). Data are expressed as means ± SD. All parameters at *day 4* were compared with *day 11* using a paired *t* test (*$P < 0.05$; **$P < 0.01$). *F*: micro-CT and flexiVent data were then correlated using a Spearman matrix. The color bar evidenced high positive correlations in red, whereas negative trends were shown in blue. For each correlation, the $R_{Spearman}$ has been reported in each box. C_{rs}, dynamic compliance; C_{st}, static compliance; CT, computed tomography; E_{rs}, elastance; IC, inspiratory capacity; 4-D, four-dimensional; FRC, functional residual capacity; *G*, lung tissue damping; *H*, lung tissue elastance; R_{rs}, resistance; V_t, tidal volume.

As expected, also FRC corresponding to the residual volume of air at the end of expiration significantly increased from 4 to 11 days for each pup ($P < 0.01$, Fig. 3*A*), concurrently with lung volumes expansion.

Tidal volume, which represents the amount of air inhaled or exhaled in a single tidal breath, was constant at the two timepoints of observation (Fig. 3*B*). However, breathing rates expressed as breaths per minute (brpm, Fig. 3*C*) were significantly increased at *day 11* compared with 4 days ($P < 0.05$). Thus, although tidal volumes were not subject to considerable variation in this growing period, minute ventilation, i.e., the volume of air movement in a minute, significantly increased at *day 11* ($P < 0.01$, Fig. 3*D*) compared with *day 4*. When normalized by body weight, however, minute ventilation/kg did not change in term neonate rabbits (Fig. 3*E*).

FlexiVent Data

As it is a terminal procedure, in this study, we only evaluated flexiVent data on *day 11*.

Dynamic resistance and compliance (R_{rs} and C_{rs}) are the most reported outcomes to assess lung function, meaning the level of constriction in the lungs and the ease with which the respiratory system can be extended, respectively. Elastance (E_{rs}) captures the elastic stiffness of the respiratory system at the ventilation frequency and corresponds to the reciprocal of the compliance.

Table 3 also shows inspiratory capacity (IC), which assesses the amount of air that can be actively inhaled at the end of a full inspiration and static compliance (C_{st}), which is derived from a pressure-volume relationship spanning over the entire inspiratory capacity.

To distinguish between the airway and tissue mechanics, airway resistance, tissue damping and tissue elastance were also reported. Tissue damping (*G*) relates to tissue resistance and reflects the energy dissipation in the alveoli, contrarily to tissue elastance (*H*), which reflects the energy conservation in the alveoli. Airway resistance (R_n), finally, represents the resistance of the central or conducting airways.

Table 3. *flexiVent data assessed at day 11*

	Parameter	Value
Static measurements		
Inspiratory capacity, mL	IC	3.19 ± 0.67
Static compliance, mL/cmH_2O·kg	C_{st}	0.32 ± 0.05
Forced oscillation		
Tissue damping, cmH_2O/mL	*G*	0.96 ± 0.21
Tissue elastance, cmH_2O/mL	*H*	3.36 ± 0.64
Airway resistance, cmH_2O·s/mL	R_n	0.06 ± 0.01
Single-frequency FOT		
Dynamic compliance, mL/cmH_2O·kg	C_{rs}	0.26 ± 0.05
Dynamic elastance, cmH_2O·kg/mL	E_{rs}	3.92 ± 0.7
Resistance, cmH_2O·s/mL	R_{rs}	0.19 ± 0.04

Values are means ± SD; $n = 6$. FOT, forced oscillation technique.

Micro-CT results on *day 11* and flexiVent were compared by a Spearman matrix (Fig. 3*F*). Good correlations, both positive and negative, were found between CT outcomes and flexiVent parameters, reaching Spearman scores higher than |0.7|, except for air-to-tissue ratio, which did not correlate with any of the flexiVent parameters.

IC, C_{rs}, and C_{st} positively correlated with FRC, V_t, and minute ventilation ($R_{Spearman} > 0.77$, $P < 0.05$). Resistance, tissue damping, and tissue elastance displayed, instead, a negative correlation with tidal volume, suggesting that lung tissue resistance may impair air exchange during normal breathing.

Histomorphometric Analysis

Histomorphological analysis of neonatal rabbits' lung parenchyma on *days 4* and *11* after birth, revealed an increasing number of newly formed septa replacing the preexisting primary septa. These structures subdivided the air spaces into smaller units, the alveoli, further enlarging the gas-exchange surface (Fig. 4*A*). The progression of lung development was documented by a significant increase in RAC value ($P < 0.001$, Fig. 4*B*), despite there being no significant change in the percentage of tissue density (TD) detected within the lung parenchyma (Fig. 4*C*).

DISCUSSION AND CONCLUSIONS

Computed tomography plays a key role as a noninvasive technology in different research fields, especially for the assessment of lung diseases in either clinical or preclinical settings.

Clinical diagnosis of several respiratory diseases is currently based on high-resolution computed tomography (HRCT), and although the most used system (visual scoring) depends on radiologists' experience (23, 24), clear guidelines are available. In contrast, a wide variation exists in preclinical applications, where unbiased operator-independent quantitative evaluations of lung function are poorly described. Micro-CT data and protocols are still scarce both for acquisition and quantification of lung CT scans in free-breathing animals; in most studies, in fact, the end-expiration phase is usually the only one quantified, since it usually produces the "best-quality" image generated during a tidal breathing.

A safe and reliable anesthesia protocol for longitudinal micro-CT quantification of lung function in newborn rabbits is lacking. In contrast to rodents, neonatal rabbits at birth are in the early to middle alveolar stage of lung development with mature surfactant and antioxidant systems, similar to newborn human infants (9, 25, 26); they thus present a great opportunity to study lung physiology and pathophysiology (8–11) in a small animal model (2). However, in this model, anesthesia is particularly challenging since newborn rabbits have a limited reserve capacity in most physiologic systems. They are highly dependent on heart rate to maintain cardiac output and blood pressure and have less functional contractile tissue, limited cardiac reserve, and low ventricular compliance compared with adults. Anatomic differences such as large tongue and less rigid airway cartilage can facilitate upper airway obstructions. The ribcage is more pliable and the intercostal muscles weaker than adults, increasing the risk of airway collapse and respiratory fatigue, thus predisposing them to rapid desaturation and hypoxemia. Thermoregulation is also impaired and the large body surface area relative to body weight, minimal fat reserve, and the absence of fur make them extremely vulnerable to hypothermia. The overall risks of anesthetic and sedation-related deaths in rabbits is 1.39% (27).

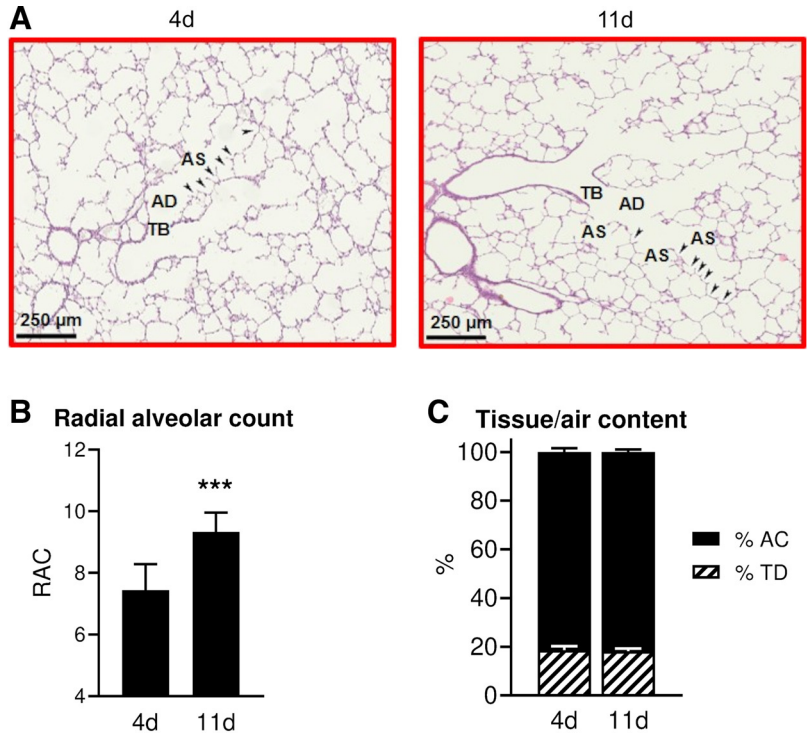

Figure 4. Histomorphometric analysis of term rabbit pups' development. *A*: representative images of the lung parenchyma 4 and 11 days after birth (scale bar 250 µm) showing different numbers of alveoli (arrowheads) composing the alveolar sacs (AS) at both timepoints. Terminal bronchioles (TB) and alveolar ducts (AD) are also indicated. *B*: the histogram shows the mean value of the radial alveolar count (RAC) measured at the two timepoints. The paired *t* test was used to compare RAC between 4 and 11 days (***$P < 0.001$). *C*: percentages of tissue and air within the area occupied by the lung section after removal of bronchi and blood vessels. Percentages of tissue and air at *day 4* were compared with *day 11* by two-way ANOVA followed by Tukey's test without demonstrating any statistical significance. Data are expressed as means ± SD.

In this study, we tested three different anesthetic protocols for longitudinal micro-CT imaging at *days 4* and *11* after birth.

Isoflurane is a common gas agent used for preclinical imaging due to its manageability, quick sedation, and rapid recovery times (1, 28). However, in newborn rabbits, an evident depression of tidal breathing associated with struggling and breath holding was observed. When administered alone, it might irritate airways and eyes even at low concentrations, provoking stress and anxiety and finally inducing apnea (29). Thus, although the above-mentioned protocol proved very simple and was applied for longitudinal micro-CT studies on rabbit neonates (2), a unique image dataset, representing an average between the inspiratory and the expiratory phase, could be acquired, precluding any micro-CT lung-function measurements.

On the other hand, even though we have shown that Keta and Xyla could be a feasible solution to derive lung-function parameters from micro-CT scans, breathing rate was affected, producing low rates and long end-expiration phases, and altering the normal breathing pattern and the subsequent functional analyses. Moreover, our internal Animal Welfare Body deemed this anesthesia protocol not fully in compliance with animal welfare requirements due to long recovery times and deep sedation observed.

A further step toward optimal sedation of newborn rabbits was achieved by combining Dex with very low concentrations of Iso (1% in oxygen) delivered using a facemask.

Dex is recognized to alleviate stress, induce fast relaxation, and predispose pups to receive isoflurane (30, 31). This approach proved safe, as revealed by monitoring of vital parameters. As expected, during anesthesia, heart rate slowed down significantly, whereas blood oxygenation was stable above 98%, since oxygen was supplied after scan acquisition. Moreover, this protocol produced rapid myorelaxation and stabilization of breathing rate, thus improving the quality of reconstructed micro-CT scans. The generation of two distinctive datasets, corresponding to end-inspiration (P01) and end-expiration (P02) phase, provided a fundamental tool for extracting data crucial to fully describing lung parenchyma changes.

Air content, FRC, and air-to-tissue ratio significantly increased from 4 to 11 days, denoting an improved lung function, which might reflect the alveolar development, whereas no changes were measured in the tissue component.

We considered the minute ventilation a dynamic and more informative parameter, consisting in the air flowing in the lung in a minute, since it has been reported that newborn mammals tend to augment breathing frequency, rather than tidal volume, to achieve higher levels of minute ventilation adequate for their metabolic needs (32).

As expected, minute ventilation significantly increased at *day 11* compared with baseline, despite it resulted constant if normalized on body weight.

Although understanding the postnatal development of the respiratory system is beyond the scope of the present study and further evaluations with multiple timepoints are required, these data support an alveolar development in line with the somatic growth of newborn rabbits, highlighting that micro-CT imaging, following an optimal anesthesia protocol, may provide a unique tool for longitudinal measures in the same subject.

A significant increase in RAC score was observed 11 days after birth evidencing the development of lung parenchyma, corroborating the significant increase measured in FRC by micro-CT.

Furthermore, to investigate the correlation between micro-CT functional analyses and the mechanics of respiratory system, lung-function testing was performed at *day 11*. As shown in the Spearman matrix, among the CT parameters, FRC and minute ventilation positively correlated with IC and static or dynamic compliance by flexiVent, indicating improved ability of the lung to stretch and expand. On the contrary, resistance and elastance related to the respiratory system (R_{rs} and E_{rs}) and the tissue component (G and H) negatively correlated with the micro-CT data.

To summarize, in this study, we set up and validated a safe and suitable anesthesia protocol in neonatal rabbits that can be used for different veterinary applications. In particular, preterm rabbit pups exposed to hyperoxia are becoming a model of reference for studying one of the most relevant neonatal diseases, bronchopulmonary dysplasia (BPD) (2, 8). A relevant next step will be the successful application of this anesthesia protocol to the aforementioned BPD model for performing longitudinal studies similar to the one described in this manuscript.

Moreover, for the first time, lung-function parameters were derived from longitudinal micro-CT images in newborn rabbits. We highlighted the important role of the anesthesia for CT imaging in neonates and how these parameters can be measured.

This study opens up the possibility of longitudinally measuring lung-function development in the same subject. Since each neonate is different in terms of lung development from other rabbit pups, the evaluation of lung function with respect to baseline offered a unique chance to dramatically reduce the intraexperimental variability and the number of pups needed to produce statistically significant results.

SUPPLEMENTAL DATA

Supplemental Fig. S1: https://doi.org/10.6084/m9.figshare.15098469.

Supplemental Fig. S2: https://doi.org/10.6084/m9.figshare.15099966.

Supplemental Fig. S3: https://doi.org/10.6084/m9.figshare.15100893.

Supplemental Table S1: https://doi.org/10.6084/m9.figshare.15101181.

GRANTS

This work was funded by Chiesi Farmaceutici S.p.A. (to L.C., C.C., F.S., and F.F.S.).

DISCLOSURES

L.C., C.C., F.S., and F.F.S. are employees of Chiesi Farmaceutici, S.p.A., which supported the research work. None of the other authors has any conflicts of interest, financial or otherwise, to disclose.

AUTHOR CONTRIBUTIONS

E.F., L.C., and F.F.S. conceived and designed research; E.F., L.C., and C.C. performed experiments; E.F. and L.L. analyzed data; E.F., L.L., L.C., L.R., and F.F.S. interpreted results of experiments; E.F. prepared figures; E.F., L.L., L.C., L.R., and F.F.S. drafted manuscript; L.C., F.S., F.P., and F.F.S. edited and revised manuscript; E.F., L.L., L.C., C.C., F.S., L.R., F.P., and F.F.S. approved final version of manuscript.

REFERENCES

1. **Ruscitti F**, **Ravanetti F**, **Bertani V**, **Ragionieri L**, **Mecozzi L**, **Sverzellati N**, **Silva M**, **Ruffini L**, **Menozzi V**, **Civelli M**, **Villetti G**, **Stellari F.** Quantification of lung fibrosis in IPF-like mouse model and pharmacological response to treatment by micro-computed tomography. *Front Pharmacol* 11: 1117, 2020. doi:10.3389/fphar.2020.01117.
2. **Salaets T**, **Aertgeerts M**, **Gie A**, **Vignero J**, **De Winter D**, **Regin Y**, **Jimenez J**, **Vande Velde G**, **Allegaert K**, **Deprest J**, **Toelen J.** Preterm birth impairs postnatal lung development in the neonatal rabbit model. *Respir Res* 21: 1–13, 2020. doi:10.1186/s12931-020-1321-6.
3. **Raghu G**, **Remy-Jardin M**, **Myers JL**, **Richeldi L**, **Ryerson CJ**, **Lederer DJ** et al**.** Diagnosis of idiopathic pulmonary fibrosis. An official ATS/ERS/JRS/ALAT clinical practice guideline. *Am J Respir Crit Care Med* 198: e44–e68, 2018. doi:10.1164/rccm.201807-1255ST.
4. **Colombi D**, **Dinkel J**, **Weinheimer O**, **Obermayer B**, **Buzan T**, **Nabers D**, **Bauer C**, **Oltmanns U**, **Palmowski K**, **Herth F**, **Kauczor HU**, **Sverzellati N**, **Kreuter M**, **Heussel CP.** Research article: visual vs fully automatic histogram-based assessment of idiopathic pulmonary fibrosis (IPF) progression using sequential multidetector computed tomography (MDCT). *PLoS One* 10: e0130653, 2015. doi:10.1371/journal.pone.0130653.
5. **Teplov A**, **Tabata K**, **Fu X**, **Uraoka N**, **Roehrl MH**, **Ntiamoah P**, **Humm JL**, **Sirintrapun SJ**, **Murray MP**, **Shia J**, **Travis WD**, **Brogi E**, **Hameed M**, **Yagi Y.** Development of standard operating procedure (SOP) of micro-computed tomography (micro-CT) in pathology. *Diagn Pathol* 5, 2019. doi:10.17629/www.diagnosticpathology.eu-2019-5:273.
6. **Schambach SJ**, **Bag S**, **Schilling L**, **Groden C**, **Brockmann MA.** Application of micro-CT in small animal imaging. *Methods* 50: 2–13, 2010. doi:10.1016/j.ymeth.2009.08.007.
7. **Ford NL**, **McCaig L**, **Jeklin A**, **Lewis JF**, **Veldhuizen RAW**, **Holdsworth DW**, **Drangova M.** A respiratory-gated micro-CT comparison of respiratory patterns in free-breathing and mechanically ventilated rats. *Physiol Rep* 5: e13074, 2017. doi:10.14814/phy2.13074.
8. **D'Angio CT**, **Ryan RM.** Animal models of bronchopulmonary dysplasia. The preterm and term rabbit models. *Am J Physiol Lung Cell Mol Physiol* 307: L959–L969, 2014. doi:10.1152/ajplung.00228.2014.
9. **Kamaruzaman NA**, **Kardia E**, **Kamaldin NA**, **Latahir AZ**, **Yahaya BH.** The rabbit as a model for studying lung disease and stem cell therapy. *Biomed Res Int* 2013: 691830, 2013. doi:10.1155/2013/691830.
10. **Van der Veeken L**, **Grönlund S**, **Gerdtsson E**, **Holmqvist B**, **Deprest J**, **Ley D**, **Bruschettini M.** Long-term neurological effects of neonatal caffeine treatment in a rabbit model of preterm birth. *Pediatr Res* 87: 1011–1018, 2020. doi:10.1038/s41390-019-0718-8.
11. **Keir S**, **Page C.** The rabbit as a model to study asthma and other lung diseases. *Pulm Pharmacol Ther* 21: 721–730, 2008. doi:10.1016/j.pupt.2008.01.005.
12. **Salaets T**, **Gie A**, **Jimenez J**, **Aertgeerts M**, **Gheysens O**, **Velde GV**, **Koole M**, **Murgia X**, **Casiraghi C**, **Ricci F**, **Salomone F**, **Villetti G**, **Allegaert K**, **Deprest J**, **Toelen J.** Local pulmonary drug delivery in the preterm rabbit: feasibility and efficacy of daily intratracheal injections. *Am J Physiol Lung Cell Mol Physiol* 316: L589–L597, 2019. doi:10.1152/ajplung.00255.2018.
13. **Gie A**, **Regin Y**, **Salaets T**, **Casiraghi C**, **Salomone F**, **Deprest J**, **Vanoirbeek J**, **Toelen J.** Intratracheal budesonide/surfactant attenuates hyperoxia-induced lung injury in preterm rabbits. *Am J Physiol Lung Cell Mol Physiol* 319: L949–L956, 2020. doi:10.1152/ajplung.00162.2020.
14. **Holden D.** Paediatric patients. In: *BSAVA Manual of Canine and Feline Anaesthesia and Analgesia*. Gloucester, UK: British Small Animal Veterinary Association, 2007, p. 296–302.
15. **Dutta S**, **Sengupta P.** Rabbits and men: relating their ages. *J Basic Clin Physiol Pharmacol* 29: 427–435, 2018. doi:10.1515/jbcpp-2018-0002.
16. **Bayne K.** Revised Guide for the care and use of laboratory animals available. American Physiological Society. *Physiologist* 39: 208–211, 1996.
17. **Du Sert NP**, **Hurst V**, **Ahluwalia A**, **Alam S**, **Avey MT**, **Baker M**, **Browne WJ**, **Clark A**, **Cuthill IC**, **Dirnagl U**, **Emerson M**, **Garner P**, **Holgate ST**, **Howells DW**, **Karp NA**, **Lazic SE**, **Lidster K**, **MacCallum CJ**, **Macleod M**, **Pearl EJ**, **Petersen OH**, **Rawle F**, **Reynolds P**, **Rooney K**, **Sena ES**, **Silberberg SD**, **Steckler T**, **Würbel H.** The arrive guidelines 2.0: updated guidelines for reporting animal research. *PLoS Biol* 18: e3000410, 2020. doi:10.1371/journal.pbio.3000410.
18. **Ford NL**, **Martin EL**, **Lewis JF**, **Veldhuizen RAW**, **Drangova M**, **Holdsworth DW.** In vivo characterization of lung morphology and function in anesthetized free-breathing mice using micro-computed tomography. *J Appl Physiol (1985)* 102: 2046–2055, 2007. doi:10.1152/japplphysiol.00629.2006.
19. **Emery JL**, **Mithal A.** The number of alveoli in the terminal respiratory unit of man during late intrauterine life and childhood. *Arch Dis Child* 35: 544–547, 1960. doi:10.1136/adc.35.184.544.
20. **Cooney TP**, **Thurlbeck WM.** The radial alveolar count method of Emery and Mithal: a reappraisal 1- postnatal lung growth. *Thorax* 37: 572–579, 1982. doi:10.1136/thx.37.8.572.
21. **Cooney TP**, **Thurlbeck WM.** The radial alveolar count method of Emery and Mithal: a reappraisal 2-intrauterine and early postnatal lung growth. *Thorax* 37: 580–583, 1982. doi:10.1136/thx.37.8.580.
22. **Elhafez E**, **Mohamed G**, **Hussein M.** Development of the respiratory acinus in the rabbit lung. *Recent Res Med Med Chem* 1: 14–17, 2012. http://www.wseas.us/e-library/conferences/2012/Kos/MEDICAL/MEDICAL-12.pdf.
23. **Lynch DA**, **Sverzellati N**, **Travis WD**, **Brown KK**, **Colby TV**, **Galvin JR**, **Goldin JG**, **Hansell DM**, **Inoue Y**, **Johkoh T**, **Nicholson AG**, **Knight SL**, **Raoof S**, **Richeldi L**, **Ryerson CJ**, **Ryu JH**, **Wells AU.** Diagnostic criteria for idiopathic pulmonary fibrosis: a Fleischner Society White Paper. *Lancet Respir Med* 6: 138–153, 2018. doi:10.1016/S2213-2600(17)30433-2.
24. **Ochiai M**, **Hikino S**, **Yabuuchi H**, **Nakayama H**, **Sato K**, **Ohga S**, **Hara T.** A new scoring system for computed tomography of the chest for assessing the clinical status of bronchopulmonary dysplasia. *J Pediatr* 152: 90–95, 2008. doi:10.1016/j.jpeds.2007.05.043.
25. **Kovar J**, **Sly PD**, **Willet KE.** Postnatal alveolar development of the rabbit. *J Appl Physiol (1985)* 93: 629–635, 2002. doi:10.1152/japplphysiol.01044.2001.
26. **Frank L**, **Sosenko IR.** Prenatal development of lung antioxidant enzymes in four species. *J Pediatr* 110: 106–110, 1987. doi:10.1016/S0022-3476(87)80300-1.
27. **Brodbelt DC**, **Blissitt KJ**, **Hammond RA**, **Neath PJ**, **Young LE**, **Pfeiffer DU**, **Wood JLN.** The risk of death: the confidential enquiry into perioperative small animal fatalities. *Vet Anaesth Analg* 35: 365–373, 2008. doi:10.1111/j.1467-2995.2008.00397.x.
28. **Mecozzi L**, **Mambrini M**, **Ruscitti F**, **Ferrini E**, **Ciccimarra R**, **Ravanetti F**, **Sverzellati N**, **Silva M**, **Ruffini L**, **Belenkov S**, **Civelli M**, **Villetti G**, **Stellari F.** In-vivo lung fibrosis staging in a bleomycin-mouse model: a new micro-CT guided densitometric approach. *Sci Rep* 10: 18735, 2020. doi:10.1038/s41598-020-71293-3.
29. **Flecknell P.** Anaesthesia of Common Laboratory Species: Special Considerations. In: *Laboratory Animal Anaesthesia* (3rd ed.). New York: Academic Press, 2009, p. 181–241.
30. **González-Gil A**, **Villa A**, **Millán P**, **Martínez-Fernández L**, **Illera JC.** Effects of dexmedetomidine and ketamine-dexmedetomidine with and without buprenorphine on corticoadrenal function in rabbits. *J Am Assoc Lab Anim Sci* 54: 299–303, 2015.
31. **Ferrini E**, **Mecozzi L**, **Corsi L**, **Ragionieri L**, **Donofrio G**, **Stellari FF.** Alfaxalone and dexmedetomidine as an alternative to gas anesthesia for micro-CT lung imaging in a bleomycin-induced pulmonary fibrosis murine model. *Front Vet Sci* 7: 588592, 2020. doi:10.3389/fvets.2020.588592.
32. **Mortola JP.** How to breathe? Respiratory mechanics and breathing pattern. *Respir Physiol Neurobiol* 261: 48–54, 2019. doi:10.1016/j.resp.2018.12.005.